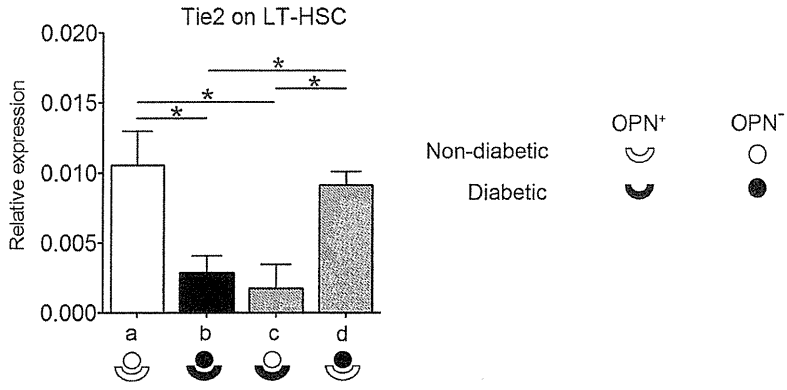

Fig. 8. Expression of Tie2 on LT-HSCs in intrabone marrow-bone marrow transplantation (IBM-BMT) mice. Mixture of nondiabetic (*a* and *c*) or diabetic (*b* and *d*) OPN^+ cells and nondiabetic (*a* and *d*) or diabetic (*b* and *c*) OPN^- cells were transplanted into the left tibia of mice. mRNA expression of Tie2 on LT-HSCs at 7 days after IBM-BMT. The values are means ± SD for $n = 4-5$ mice. $^*P < 0.05$, compared with other groups.

in the diabetic mice. Hyperactivity of osteoclasts in the diabetic state has been shown in a previous study (24).

The present results also revealed that the expression of N-cadherin on LT-HSCs and the expression of β_1-integrin on osteoblastic niche cells were reduced in diabetic mice. As N-cadherin-mediated adhesion mediates the slow cycling and quiescence of HSCs (1, 11, 12), and β_1-integrin is essential for the interaction between bone marrow niche cells and HSCs and for regulating the initial self-renewing HSC division and survival (10), our findings suggest that HSCs failed to maintain quiescence, self-renewal, and survival under diabetic conditions.

The Wnt signaling cascade is triggered upon binding to a coreceptor complex, including Fzd and LRP5/6 (2, 8, 15, 29). Wnt, Fzd, and Dkk are included in the β-catenin phosphorylation complex, which leads to β-catenin degradation, and Dkk binds to and inactivates the signaling from LRP5/6 receptors. Wnt/β-catenin signaling may play a crucial role in the maintenance of the self-renewal activity in bone marrow. In the present study, we showed that both the LRP6 expression on LT-HSCs and the β-catenin expression on LH-HSCs were reduced in diabetic mice, suggesting that diabetes impairs the Wnt/β-catenin pathway, resulting in abnormalities in the reconstituting of HSCs.

Chemokines and their receptors control the behavior of HSCs by regulating the migration, homing, and release of HSCs within the bone marrow. The importance of CXCL12/CXCR4 signaling was previously demonstrated in $CXCL12^{-/-}$ and $CXCR4^{-/-}$ mice (33, 37), which have a severe defect in their bone marrow myeloid progenitors. We herein demonstrated that diabetes induced the depletion of CXCL12 expression by osteoblastic niche cells, suggesting that there is an impaired interaction between osteoblastic niche cells and LT-HSCs in the bone marrow in diabetic mice.

Our in vitro coculture of LT-HSCs and osteoblastic niche cells in normal and high-glucose media aimed to mimic the diabetic and nondiabetic microenvironments in the bone marrow niche. The morphological features of the interactions between osteoblastic niche cells and LT-HSCs in the coculture experiments were shown to be similar to the in vivo localization of osteoblastic niche cells and LT-HSCs in the bone marrow sections. Furthermore, the staining pattern was the same between nondiabetic and diabetic mice, suggesting that the surface phenotype of osteoblastic niche cells and LT-HSCs may remain in diabetic mice, separate from their functional abnormalities. In coculture experiments, osteoblastic niche cells derived from nondiabetic mice were found to adhere to the culture plate for 7 days under normoglycemic, but not hyperglycemic, conditions. The reverse was true for osteoblastic niche cells derived from diabetic mice, suggesting that such cells adapt to higher glucose concentrations. The survival frequency of LT-HSCs paralleled the existence of osteoblastic niche cells. Therefore, our coculture experiments provide an adequate microenvironment for keeping LT-HSCs in contact with osteoblastic niche cells and for maintaining the stemness for at least 7 days. Attempts have previously been made to reconstitute a bone marrow niche using three-dimensional (17, 28) or low oxygen tension (13) coculture systems. However, as shown here, a conventional two-dimensional coculture appears to be sufficient.

The coculture experiments showed the same abnormalities in the LT-HSC expression of N-cadherin, β-catenin, and Tie2 seen in vivo in the diabetic mice. The use of different coculture combinations of LT-HSCs and osteoblastic niche cells led to several important findings: nondiabetic LT-HSCs with diabetic osteoblastic niche cells led to reduced expression of these molecules, perhaps through impairment of the self-renewal, survival, and quiescence of HSCs. Most interestingly, the in vitro exposure of diabetic LT-HSCs to nondiabetic osteoblastic niche cells successfully reversed these abnormalities in expression. Although it is known that diabetes induces impaired hematopoietic stem/progenitor cell mobilization and repopulation by altering the functions of the bone marrow niche (7, 27), no previous studies have shown the effects of the replacement of bone marrow niche cells on their partner HSCs. Our in vivo IBM-BMT experiments revealed that the replacement of osteoblastic niche cells could successfully reverse the abnormalities in LT-HSCs caused by diabetes.

In summary, we have demonstrated that diabetes induces impairments in the expression of molecules on both LT-HSCs and osteoblastic niche cells, which are essential for maintaining the quiescence and reconstitution of HSCs in the bone marrow niche. Normal LT-HSCs displayed abnormal expression of these molecules when exposed to diabetic osteoblastic niche cells, but this abnormality could be reversed after exposure to nondiabetic osteoblastic niche cells. Although it is not known at present how diabetic metabolism impairs the osteoblastic niche cells, the present results provide important information for the treatment of diabetes-induced HSC abnormalities, which could include the replacement of bone marrow niche cells.

ACKNOWLEDGMENTS

We thank Susumu Ikehara and Ming Li for support for IBM-BMT.

GRANTS

This work was supported by Grant-in-Aid for Scientific Research 23592223 (to K. Iba) and 21390054 (to M. Fujimiya) from the Ministry of Education, Culture, Sports, Science, and Technology, Japan.

DISCLOSURES

No conflicts of interest, financial or otherwise, are declared by the author(s).

AUTHOR CONTRIBUTIONS

Author contributions: H.C. and K.A. performed experiments; H.C., K.A., K.I., and K.N. analyzed data; H.C., K.A., K.I., K.N., and T.Y. interpreted results of experiments; H.C. and K.A. prepared figures; H.C., K.A., and M.F. drafted manuscript; K.A. and M.F. approved final version of manuscript; K.I., T.Y., and M.F. conception and design of research.

REFERENCES

1. **Arai F, Suda T.** Maintenance of quiescent hematopoietic stem cells in the osteoblastic niche. *Ann NY Acad Sci* 106: 41–53, 2007.
2. **Baron R, Rawadi G.** Targeting the Wnt/beta-catenin pathway to regulate bone formation in the adult skeleton. *Endocrinology* 148: 2635–2643, 2007.
3. **Bar-Shavit Z.** The osteoclast: a multinucleated, hematopoietic-origin, bone-resorbing osteoimmune cell. *J Cell Biochem* 102: 1130–1139, 2007.
4. **Chan L, Terashima T, Fujimiya M, Kojima H.** Chronic diabetic complications: the body's adaptive response to hyperglycemia gone awry? *Trans Am Clin Climatol Assoc* 117: 341–351, 2006.
5. **Ehninger A, Trumpp A.** The bone marrow stem cell niche grows up: mesenchymal stem cells and macrophages move in. *J Exp Med* 208: 421–428, 2011.
6. **Fadini GP, Boscaro E, de Kreutzenberg S, Agostini C, Seeger F, Dimmeler S, Zeiher A, Tiengo A, Avogaro A.** Time course and mechanisms of circulating progenitor cell reduction in the natural history of type 2 diabetes. *Diabetes Care* 33: 1097–1102, 2010.
7. **Ferraro F, Lymperi S, Méndez-Ferrer S, Saez B, Spencer JA, Yeap BY, Masselli E, Graiani G, Prezioso L, Rizzini EL, Mangoni M, Rizzoli V, Sykes SM, Lin CP, Frenette PS, Quaini F, Scadden DT.** Diabetes impairs hematopoietic stem cell mobilization by altering niche function. *Sci Transl Med* 3: 101–104, 2011.
8. **Fleming HE, Janzen V, Lo Celso C, Guo J, Leahy KM, Kronenberg HM, Scadden DT.** Wnt signaling in the niche enforces hematopoietic stem cell quiescence and is necessary to preserve self-renewal in vivo. *Cell Stem Cell* 2: 274–283, 2008.
9. **Fujimiya M, Kojima H, Ichinose M, Arai R, Kimura H, Kashiwagi A, Chan L.** Fusion of proinsulin-producing bone marrow-derived cells with hepatocytes in diabetes. *Proc Natl Acad Sci USA* 104: 4030–4035, 2007.
10. **Gottschling S, Saffrich R, Seckinger A, Krause U, Horsch K, Miesala K, Ho AD.** Human mesenchymal stromal cells regulate initial self-renewing divisions of hematopoietic progenitor cells by a beta1-integrin-dependent mechanism. *Stem Cells* 25: 798–806, 2007.
11. **Haug JS, He XC, Grindley JC, Wunderlich JP, Gaudenz K, Ross JT, Paulson A, Wagner KP, Xie Y, Zhu R, Yin T, Perry JM, Hembree MJ, Redenbaugh EP, Radice GL, Seidel C, Li L.** N-cadherin expression level distinguished reserved versus primed states of hematopoietic stem cells. *Cell Stem Cells* 2: 367–379, 2008.
12. **Hosokawa K, Arai F, Yoshihara H, Iwasaki H, Nakamura Y, Gomei Y, Suda T.** Knockdown of N-cadherin suppresses the long-term engraftment of hematopoietic stem cells. *Blood* 116: 554–563, 2010.
13. **Jing D, Wobus M, Poitz DM, Bornhauser M, Ehninger G, Ordemann R.** Oxygen tension plays a critical role in the hematopoieticmicroenvironment in vitro. *Hematologica* 97: 331–339, 2012.
14. **Kawamoto T.** Use of a new adhesive film for the preparation of multi-purpose fresh-frozen sections from hard tissues, whole-animals, insects and plants. *Arch Histol Cytol* 66: 123–143, 2003.
15. **Kirstetter P, Anderson K, Porse BT, Jacobsen SE, Nerlov C.** Activation of the canonical Wnt pathway leads to loss of hematopoietic stem cell repopulation and multilineage differentiation block. *Nat Immunol* 7: 1048–1056, 2006.
16. **Kushida T, Inaba M, Hisha H, Ichioka N, Esumi T, Ogawa R, Iida H, Ikehara S.** Intra-bone marrow injection of allogeneic bone marrow cells: a powerful new strategy for treatment of intractable autoimmune diseases in MRL/lpr mice. *Blood* 97: 3292–3299, 2001.
17. **Leisten I, Kramann R, Ventura Ferreira MS, Bovi M, Neuss S, Ziegler P, Wagner W, Knüchel R, Schneider RK.** 3D coculture of hematopoietic stem and progenitor cells and mesenchymal stem cells in collagen scaffolds as a model of the hematopoietic niche. *Biomaterials* 3: 1736–1747, 2012.
18. **Li L, Bhatia R.** Stem cell quiescence. *Clin Cancer Res* 17: 4936–4941, 2011.
19. **Loomans CJ, de Koning EJ, Staal FJ, Rookmaaker MB, Verseyden C, de Boer HC, Verhaar MC, Braam B, Rabelink TJ, van Zonneveld AJ.** Endothelial progenitor cell dysfunction: a novel concept in the pathogenesis of vascular complications of type 1 diabetes. *Diabetes* 53: 195–199, 2004.
20. **Ma Z, Wirström T, Borg LA, Larsson-Nyrén G, Hals I, Bondo-Hansen J, Grill V, Björklund A.** Diabetes reduces β-cell mitochondria and induces distinct morphological abnormalities, which are reproducible by high glucose in vitro with attendant dysfunction. *Islets* 4: 233–242, 2012.
21. **Mayack SR, Shadrach JL, Kim FS, Wagers AJ.** Systemic signals regulate ageing and rejuvenation of blood stem cell niches. *Nature* 463: 495–500, 2010.
22. **Méndez-Ferrer S, Michurina TV, Ferraro F, Mazloom AR, Macarthur BD, Lira SA, Scadden DT, Ma'ayan A, Enikolopov GN, Frenette PS.** Mesenchymal and haematopoietic stem cells form a unique bone marrow niche. *Nature* 466: 829–834, 2010.
23. **Mercier FE, Ragu C, Scadden DT.** The bone marrow at the crossroads of blood and immunity. *Nat Rev Immunol* 12: 49–60, 2012.
24. **Motyl K, McCabe LR.** Streptozotocin, type I diabetes severity and bone. *Biol Proced Online* 11: 296–315, 2009.
25. **Ogawa M.** Differentiation and proliferation of hematopoietic stem cells. *Blood* 81: 2844–2853, 1993.
26. **Omatsu Y, Sugiyama T, Kohara H, Kondoh G, Fujii N, Kohno K, Nagasawa T.** The essential functions of adipo-osteogenic progenitors as the hematopoietic stem and progenitor cell niche. *Immunity* 33: 387–399, 2010.
27. **Orlandi A, Chavakis E, Seeger F, Tjwa M, Zeiher AM, Dimmeler S.** Long-term diabetes impairs repopulation of hematopoietic progenitor cells and dysregulates the cytokine expression in the bone marrow microenvironment in mice. *Basic Res Cardiol* 105: 703–712, 2010.
28. **Sharma MB, Limaye LS, Kale VP.** Mimicking the functional hematopoietic stem cell niche in vitro: recapitulation of marrow physiology by hydrogel-based three-dimensional cultures of mesenchymal stromal cells. *Hematologica* 97: 651–660, 2012.
29. **Suda T, Arai F.** Wnt signaling in the niche. *Cell* 132: 729–730, 2008.
30. **Tepper OM, Carr J, Allen RJ Jr, Chang CC, Lin Tanaka R CD, Gupta SM, Levine JP, Saadeh PB, Warren SM.** Decreased circulating progenitor cell number and failed mechanisms of stromal cell-derived factor-1alpha mediated bone marrow mobilization impair diabetic tissue repair. *Diabetes* 59: 1974–1983, 2010.
31. **Terashima T, Kojima H, Fujimiya M, Matsumura K, Oi J, Hara M, Kashiwagi A, Kimura H, Yasuda H, Chan L.** The fusion of bone-marrow-derived proinsulin-expressing cells with nerve cells underlies diabetic neuropathy. *Proc Natl Acad Sci USA* 102: 12525–12530, 2005.
32. **Tariq M, Masoud MS, Mehmood A, Khan SN, Riazuddin S.** Stromal cell derived factor-1alpha protects stem cell derived insulin-producing cells from glucotoxicity under high glucose conditions in-vitro and ameliorates drug induced diabetes in rats. *J Transl Med* 11: 115, 2013.
33. **Tzeng YS, Li H, Kang YL, Chen WC, Cheng WC, Lai DM.** Loss of Cxcl12/Sdf-1 in adult mice decreases the quiescent state of hematopoietic stem/progenitor cells and alters the pattern of hematopoietic regeneration after myelosuppression. *Blood* 117: 429–439, 2011.
34. **Wang DL, Wagers AJ.** Dynamic niches in the origination and differentiation of haematopoietic stem cells. *Nat Rev Mol Cell Biol* 12: 643–655, 2011.
35. **Weksberg DC, Chambers SM, Boles NC, Goodell MA.** CD150- side population cells represent a functionally distinct population of long-term hematopoietic stem cells. *Blood* 111: 2444–2451, 2008.
36. **Yamashita T, Fujimiya M, Nagaishi K, Ataka K, Tanaka M, Yoshida H, Tsuchihashi K, Shimamoto K, Miura T.** Fusion of bone marrow-derived cells with renal tubules contributes to renal dysfunction in diabetic nephropathy. *FASEB J* 26: 1559–1568, 2012.
37. **Zou YR, Kottmann AH, Kuroda M, Taniuchi I, Littman DR.** Function of the chemokine receptor CXCR4 in haematopoiesis and in cerebellar development. *Nature* 393: 595–599, 1998.

HEPATOLOGY
Official Journal of the American Association for the Study of Liver Diseases

Mesenchymal Stem Cell Therapy Ameliorates Diabetic Hepatocyte Damage in Mice by Inhibiting Infiltration of Bone Marrow–Derived Cells

Kanna Nagaishi,[1] Koji Ataka,[1] Eijiro Echizen,[1] Yoshiaki Arimura,[2] and Mineko Fujimiya[1]

Although mesenchymal stem cells (MSCs) have been implicated in hepatic injury, the mechanism through which they contribute to diabetic liver disease has not been clarified. In this study, we investigated the effects of MSC therapy on diabetic liver damage with a focus on the role of bone-marrow–derived cells (BMDCs), which infiltrate the liver, and elucidated the mechanism mediating this process. Rat bone-marrow (BM)-derived MSCs were administered to high-fat diet (HFD)-induced type 2 diabetic mice and streptozotocin (STZ)-induced insulin-deficient diabetic mice. MSC-conditioned medium (MSC-CM) was also administered to examine the trophic effects of MSCs on liver damage. Therapeutic effects of MSCs were analyzed by assessing serum liver enzyme levels and histological findings. Kinetic and molecular profiles of BMDCs in the liver were evaluated using BM-chimeric mice. Curative effects of MSC and MSC-CM therapies were similar because both ameliorated the aggravation of aspartate aminotransferase and alanine aminotransferase at 8 weeks of treatment, despite persistent hyperlipidemia and hyperinsulinemia in HFD-diabetic mice and persistent hyperglycemia in STZ-diabetic mice. Furthermore, both therapies suppressed the abnormal infiltration of BMDCs into the liver, reversed excessive expression of proinflammatory cytokines in parenchymal cells, and regulated proliferation and survival signaling in the liver in both HFD- and STZ-diabetic mice. In addition to inducing hepatocyte regeneration in STZ-diabetic mice, both therapies also prevented excessive lipid accumulation and apoptosis of hepatocytes and reversed insulin resistance (IR) in HFD-diabetic mice. *Conclusion:* MSC therapy is a powerful tool for repairing diabetic hepatocyte damage by inhibiting inflammatory reactions induced by BMDCs and IR. These effects are likely the result of humoral factors derived from MSCs. (HEPATOLOGY 2014;59:1816-1829)

The incidence of diabetes is second only to that of cancer. Type 2 diabetes (T2D) is associated with nonalcoholic fatty liver disease (NAFLD), which progresses to nonalcoholic steatohepatitis (NASH). Insulin resistance (IR), fatty acid accumulation in the liver, and proinflammatory cytokine expression are the main factors that increase susceptibility to hepatocyte damage in NASH.[1] In addition, the preva-

Abbreviations: Akt, protein kinase B; ALT, alanine aminotransferase; ANOVA, analysis of variance; AST, aspartate aminotransferase; Bcl2, B-cell lymphoma 2; BM, bone marrow; BMDC, BM-derived cell; BMT, BM transplantation; b.w., body weight; Ccr2, C-C chemokine receptor 2; C/EBPα, CCAAT/enhancer-binding protein alpha; ERK, extracellular signal-regulated kinase; FABP4, fatty-acid–binding protein 4; FACS, fluorescence-activated cell sorting; Fizz1, found in inflammatory zone 1; FoxO1, forkhead box O1; GFP, green fluorescence protein; GLUT2, glucose transporter 2; HFD, high-fat diet; HNF-4, hepatocyte nuclear factor 4; HOMA-IR, homeostasis model assessment-estimated IR; HSECs, hepatic sinusoidal endothelial cells; ICAM-1, intracellular adhesion molecule 1; IL, interleukin; IP, intraperitoneal; IR, insulin resistance; Irs-2, insulin receptor substrate 2; JNK, c-Jun amino-terminal kinase; MAPK, mitogen-activated protein kinase; MCs, mononuclear cells; MCP, monocyte chemotactic protein; Mrc1, mannose receptor C type 1; MSC, mesenchymal stem cell; MSC-CM, MSC-conditioned medium; NAFLD, nonalcoholic fatty liver disease; NASH, nonalcoholic steatohepatitis; NF-κB, nuclear factor kappa light-chain enhancer of activated B cells; PBMCs, peripheral blood mononuclear cells; PBS, phosphate-buffered saline; RBCs, red blood cells; SE, standard error; SECs, sinusoidal endothelial cells; SREBP-1c, sterol response element-binding protein 1c; STZ, streptozotocin; T2D, type 2 diabetes; TGF-β1, transforming growth factor beta 1; Tg, transgenic; TLR4, Toll-like receptor 4; TNFα, tumor necrosis factor alpha; Trop2, trophoblast cell-surface antigen 2; TUNEL, terminal deoxynucleotidyl transferase-mediated dUTP nick-end labeling.

From the [1]Second Department of Anatomy and [2]First Department of Internal Medicine, Sapporo Medical University, School of Medicine, Sapporo, Japan.

Received January 13, 2013; accepted December 12, 2013.

This work was supported, in part, by a Grant-in-Aid for Scientific Research (C) in Japan (to K.N.).

lence of elevated alanine aminotransferase (ALT) is also 3- to 4-fold higher in patients with type 1 diabetes, compared with the general population, with a marked accumulation of glycogen and steatohepatitis.[2] Therefore, the therapeutic approach for reversing hepatocyte damage as well as IR caused by diabetes is a matter of significance.

Previously, we detected proinsulin- and tumor necrosis factor alpha (TNFα)-producing abnormal cells in the bone marrow (BM) of high-fat diet (HFD)-induced and streptozotocin (STZ)-induced diabetic mice and showed that these cells migrated from the BM to infiltrate the liver.[3] In diabetes, BM-derived cells (BMDCs) infiltrate the liver excessively and subsequently produce cytotoxic chemokines or fuse with hepatocytes, causing parenchymal cells to produce proinsulin and cytotoxic TNFα, which leads to the degeneration or apoptosis of target cells.[4,5] These findings, in the context of diabetes, suggest that hyperglycemia is the primary cause of abnormal cells in BM and that infiltration of abnormal BMDCs in the liver may be the secondary cause of hepatocyte degeneration.

Intravenous transplantation of BM-derived mesenchymal stem cells (MSCs) has been demonstrated to be effective for diabetes. However, most previous studies have investigated the potential role of BM-derived MSCs in regenerating β cells and for subsequently improving hyperglycemia in type 1 or insulin deficiency diabetes models.[6,7] A limited number of reports have shown the effects of BM-derived MSCs on T2D with hepatocyte damage and IR.[8,9] Previous studies have reported that MSC therapy reversed hepatic enzyme levels in HFD-induced diabetic mice and suppressed proinflammatory cytokine expression in the liver, but MSC therapy failed to reverse obesity, hypercholesterolemia, hyperglycemia, and IR.[8] Another study showed an improvement in IR in an HFD-induced diabetes model[9]; however, rats received an STZ injection in addition to a 2-week HFD and the model was also an insulin deficiency model, rather than a hyperinsulinemia T2D model, so the therapeutic effects of MSCs were derived from pancreatic β-cell regeneration. To date, no reports have shown the effects of MSCs on IR associated with NAFLD or NASH in T2D with persistent hyperglycemia and -insulinemia.

BM-derived MSCs are known to exert immunoregulatory and antiapoptotic effects.[10] The mechanism of action underlying MSC therapy is suggested to mediate the cell complement effect by cell differentiation or various paracrine effects through trophic factors secreted by MSCs.[11] In fact, because systemic infusion of MSC-conditioned medium (MSC-CM) has been shown to ameliorate hepatocellular death and stimulate hepatocyte regeneration in a rat model of fulminant hepatic failure,[12] the mechanism of action of systemically injected MSCs might be the result of their released humoral factors. This hypothesis is conceivable because the number of MSCs logged after systemic injection is remarkably small, considering their powerful therapeutic effects.

In this study, we aimed to investigate the following effects resulting from intravenous administration of MSCs, which contributed to a common, distinctive pathogenesis in liver of mice in an HFD-induced T2D model and an STZ-injected insulin deficiency model: (1) suppression of abnormal BMDC infiltration into the liver; (2) amelioration of hepatocyte degeneration induced by proinflammatory cytokine expression and subsequent apoptosis; (3) enhancement of hepatocyte regeneration; and (4) reduction of IR associated with lipid accumulation and proinflammatory cytokine expression in the liver. To clarify the therapeutic effects of MSC-derived trophic factors, effects of MSC infusion were compared in parallel with those of MSC-CM administration. The present findings may provide new perspectives on therapeutic approaches to diabetes-induced hepatic damage.

Materials and Methods

Animals and BM Transplantation. C57BL/6J mice and C57BL/6-Tg (CAG-EGFP; green fluorescence protein-transgenic [GFP-Tg]) mice were purchased from Japan SLC (Shizuoka, Japan). GFP-BM chimeric mice were produced by lethal irradiation

Address reprint requests to: Mineko Fujimiya, M.D., Ph.D., Second Department of Anatomy, Sapporo Medical University School of Medicine, S-1, W-17, Chuo-ku, Sapporo 060-8556, Japan. E-mail: fujimiya@sapmed.ac.jp; fax: +81-11-618-4288.

View this article online at wileyonlinelibrary.com.
DOI 10.1002/hep.26975
Potential conflict of interest: Nothing to report.
Additional Supporting Information may be found in the online version of this article.

(9 Gy) and systemic injection with 4-6 × 10^6 BM cells isolated from GFP-Tg mice. Four weeks after BM transplantation (BMT), hyperglycemia was induced by feeding a HFD containing 60% lard (High-Fat Diet 32; Clea Japan Inc., Tokyo, Japan) or by a single intraperitoneal (IP) injection of STZ (150 mg/kg; Wako, Osaka, Japan) dissolved in citrate buffer (pH 4.5). Controls were fed a normal diet or treated with an IP injection of buffer. After 28 weeks of HFD feeding, mice were administered 1 × 10^4 MSCs/g body weight (b.w.) four times every 2 weeks (HFD-MSC), whereas controls received vehicle (HFD-vehicle; Fig. 1A). At 4 weeks after STZ injection, mice were administered twice with 1 × 10^4 MSCs/g b.w. every 4 weeks (STZ-MSC), whereas controls received vehicle (STZ-vehicle; Fig. 2A). This study was performed with the approval of the animal experiment committee of Sapporo Medical University (Sapporo, Japan).

Isolation, Culture, and Characterization of Rat BM-Derived MSCs. Rat MSCs were harvested from BM of 8-week-old Lewis rats (Charles River Laboratories Japan Inc., Yokohama, Japan) and cultured as described previously.[13] Immunophenotype and differentiation potential of rat MSCs were then determined (Supporting Fig. 1A,B).

Preparation of MSC-CM From Rat MSCs. Rat MSCs (2 × 10^5 cells) were seeded in 150-cm^2 culture dishes. When MSCs reached confluence, the medium was changed to serum-free medium and cultured for 24 hours. Then, the supernatant was collected and further concentrated (final concentration: 1 mg/mL) as MSC-CM by ultrafiltration using centrifugal filter units with a 10-kDa cutoff (Ultracel-10K; Millipore, Billerica, MA), following the manufacturer's instructions.

Intravenous Administration of MSCs and MSC-CM. MSCs (1 × 10^4 MSCs/g b.w. per animal suspended in 200 μL of phosphate-buffered saline [PBS]) or MSC-CM (2 mg/kg/day) were administered through the tail vein of mice after induction of diabetes (Fig. 1D). Vehicle administration was PBS for MSC therapy. We also administered MSC-CM to diabetic mice daily for 8 weeks (Fig. 2D). Vehicle administration was serum-free medium that was concentrated using the same procedure as that for the conditioned medium used for MSC-CM therapy.

Detection of Donor MSCs. HFD- and STZ-induced diabetic mice without BMT were administered MSCs labeled with PKH26 Red Fluorescent Cell Linker Kits (Sigma-Aldrich, Saint Louis, MO), sacrificed at 1, 2, or 4 weeks after MSC injection, and lung, liver, kidney, spleen, and bone were obtained. Organs were immersed in 4% paraformaldehyde, and bone was decalcified with 0.5 M of ethylenediaminetetraacetic acid (Wako, Osaka, Japan) for 2 days. Frozen sections of each organ were stained with 4',6-diamidino-2-phenylindole (Dojindo Laboratories, *Kumamoto*, Japan) at 0.1 mg/mL. Distribution of MSCs expressing red fluorescence in each organ was observed by confocal laser scanning microscopy (LSM 510; Carl Zeiss, Oberkochen, German). The ratio of MSCs distributed in each organ was determined by counting PKH26-positive cells in 20 randomly selected visual fields at 100× magnification per mouse (n = 3-5) and compensated by the number of MSCs given to each mouse.

Quantitative Analysis of the GFP-Positive Area. The mean percentage of the area occupied by GFP-positive cells in the liver of each animal was determined by sampling 20 randomly selected visual fields at 100× magnification using the NIS element BR 3.0 image analyzing system.

Isolation of GFP-Positive BMDCs From the Liver by Fluorescence-Activated Cell Sorting. GFP-positive BMDCs were isolated from the liver. Pieces of liver were removed, minced, and treated with 400 U/mL of collagenase (Wako) diluted in PBS for 30 minutes at 37°C. Dissolved tissue was further minced and filtered with a 100-μm pore cell strainer and centrifuged for 5 minutes at 300×*g*. The cell pellet was treated with red blood cell (RBC) lysis buffer (Qiagen, Venlo, the Netherlands) to remove remaining RBCs and washed with 2% fetal bovine serum in 0.1 M of PBS. GFP-positive BMDCs were isolated by fluorescence-activated cell sorting (FACS; Aria; BD Biosciences, Tokyo, Japan).

Isolation of Mononuclear Cells From Peripheral Blood. Peripheral blood mononuclear cells (PBMCs) were isolated by the Ficoll-Paque (GE Healthcare Japan, Tokyo, Japan) density-gradient separation method, following the manufacturer's instructions.

Statistical Analysis. Data are expressed as mean ± standard error (SE) values. Analysis of variance (ANOVA) was employed for multiple comparisons. Two-way repeated-measures (mixed between-within subjects) ANOVA, followed by Bonferroni's test, was used for serial assessment. Differences were considered significant at $P < 0.05$ in all two-tailed tests.

Results

Differentiation of Rat BM-Derived MSCs Into Multiple Mesenchymal Lineages. Specific surface antigens for rat MSCs were detected by FACS. CD90 was positively detected, whereas CD11b, CD31, CD43,

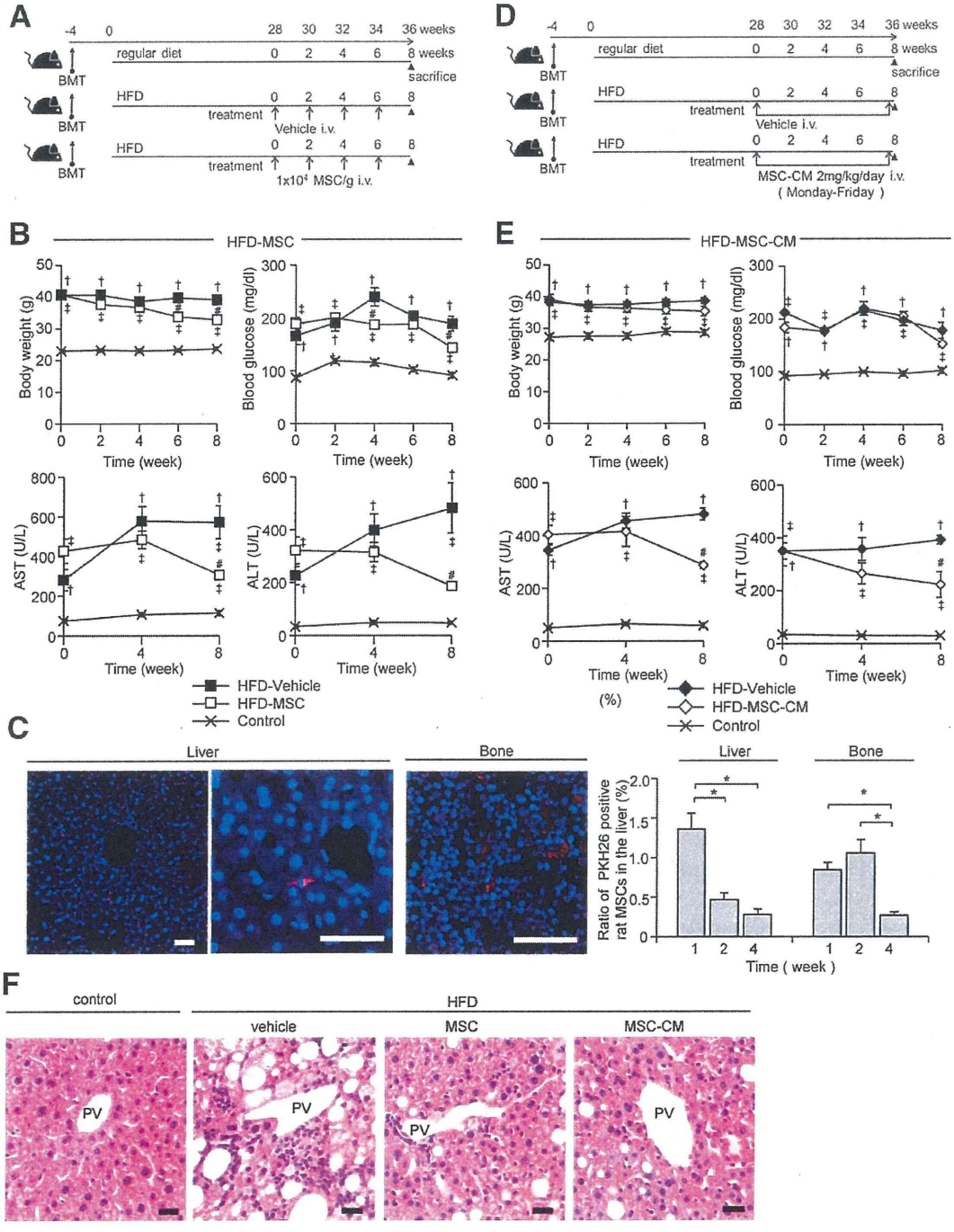

Fig. 1. Rat MSC therapy for HFD-induced diabetic mice. Protocol for MSC (A) and MSC-CM (D) therapies in HFD-diabetic mice. (B and E) Changes in body-weight and serum blood-glucose levels, AST, and ALT after beginning rMSC therapy. Data are expressed as mean ± SE values of 5-10 animals. †$P < 0.05$, HFD-vehicle versus control; ‡$P < 0.05$, HFD-MSC or HFD-MSC-CM versus control; #$P < 0.05$, HFD-MSC or HFD-MSC-CM versus HFD-vehicle. (C) Distribution of rMSCs marked with PKH26 in liver and femur of HFD mice at 1 week after initial rMSC injection are shown in left panel. Changes in the ratio of PKH26-positive cells in liver and bone at 1, 2, and 4 weeks after initial rMSC injection are shown in right panel. Bar, 50 μm. (F) Histological findings of the periportal area in the hematoxylin and eosin–stained liver section 8 weeks after initial MSC therapy. Bar, 20 μm.

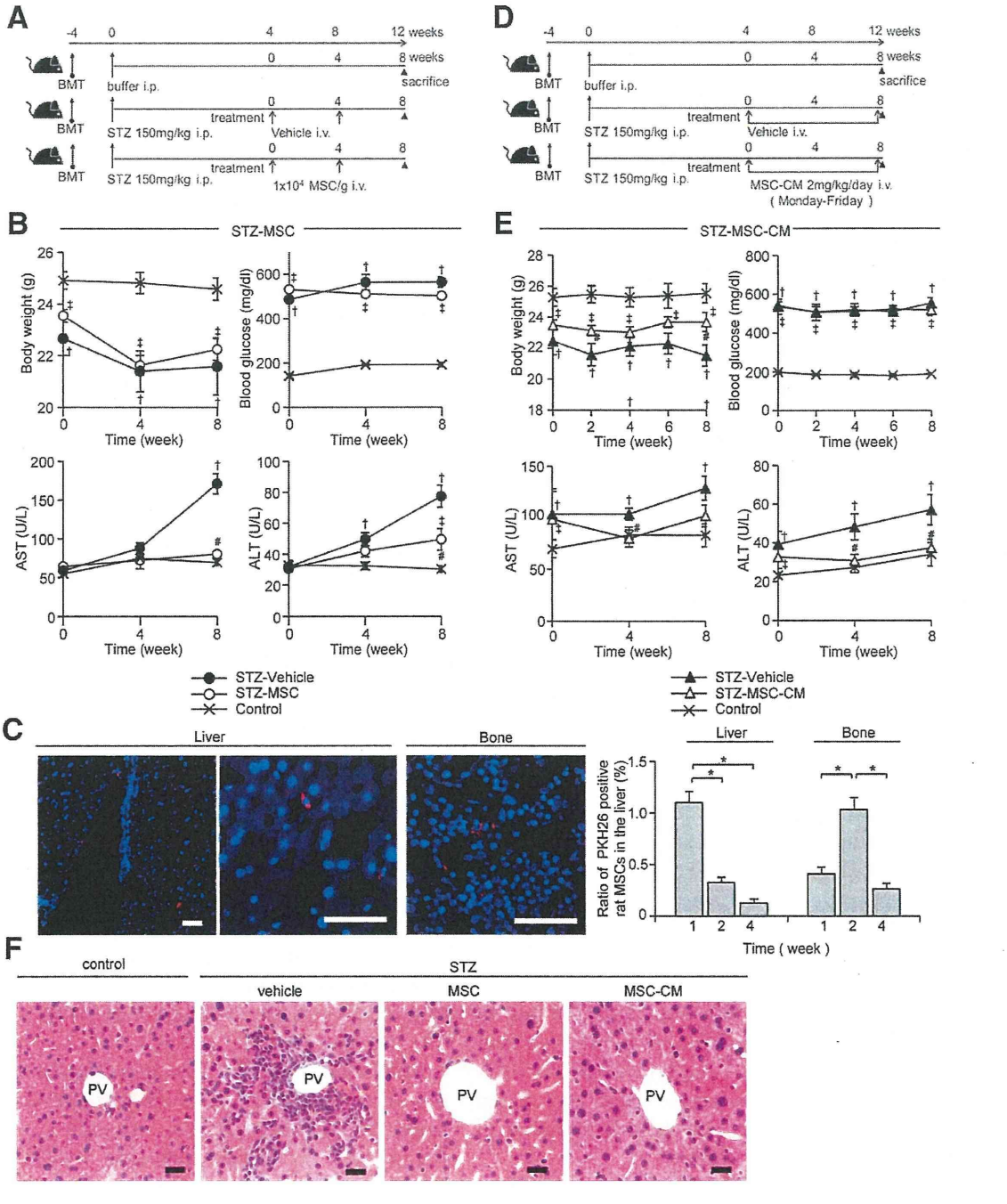

Fig. 2. Rat MSC therapy for STZ-induced diabetic mice. Protocol for MSC (A) and MSC-CM (D) therapies in STZ-diabetic mice. (B and E) Changes in body-weight and serum blood-glucose levels, AST, and ALT after beginning rMSC therapy. Data are expressed as mean ± SE values of 5-10 animals. †$P < 0.05$, STZ-vehicle versus control; ‡$P < 0.05$, STZ-MSC or STZ-MSC-CM versus control; #$P < 0.05$, STZ-MSC or STZ-MSC-CM versus STZ-vehicle. (C) Distribution of rMSCs marked with PKH26 in liver and femur of STZ mice at 1 week after initial rMSC injection were shown in the left panel. Changes in the ratio of PKH26-positive cells in liver and bone at 1, 2, and 4 weeks after initial rMSC injection are shown in right panel. Bar, 50 μm. (F) Histological findings of the periportal area in the hematoxylin and eosin-stained liver section 8 weeks after the initial MSC therapy. Bar, 20 μm.

CD44, and CD45 were negative (Supporting Fig. 1A). MSCs exhibited osteogenic, adipose, and chondrogenic differentiation ability (Supporting Fig. 1B).

MSC Therapy Prevented Liver Damage in HFD- and STZ-Diabetic Mice. MSC treatment successfully reversed hepatocyte damage caused by diabetes, as

indicated by recovery of aspartate aminotransferase (AST) and ALT levels after 8 weeks of treatment in both HFD-MSC (Fig. 1B) and STZ-MSC mice (Fig. 2B), compared to HFD- and STZ-vehicle mice, respectively. Body-weight and blood-glucose levels were mildly ameliorated in HFD-MSC mice, compared to HFD-vehicle mice (Fig. 1B); however, they were unchanged between STZ-vehicle and STZ-MSC (Fig. 2B).

Administered MSCs Detected in Liver and BM of HFD- and STZ-Diabetic Mice. PKH26-positive MSCs were detected in the periportal area and in the parenchyma of the liver, as well as around the marrow sinusoid and in the bone parenchyma in HFD-MSC and STZ-MSC mice (Figs. 1C and 2C). Detection frequency of administered MSCs was changed, depending on the time. The number of MSCs distributed in the liver decreased over time, whereas it was increased for 2 weeks after administration before decreasing thereafter in bone. However, the number of PKH26-positive MSCs detected was too small to account for the direct effect of MSCs, such as cell-cell contact or cell differentiation.

MSC-CM Therapy Prevented Liver Damage in HFD- and STZ-Diabetic Mice, Similar to MSCs. Similar to the effect of cell therapy, MSC-CM injections successfully reversed hepatocyte damage, as indicated by recovery of AST and ALT levels after 8 weeks of initial administration in HFD-diabetic mice and after 4 weeks of initial administration in STZ-diabetic mice (Figs. 1E and 2E). In contrast to cell therapy, there were no differences in body-weight or fasting blood-glucose levels between HFD-MSC-CM and HFD-vehicle mice (Fig. 1E). Body weight recovered in STZ-MSC-CM mice, whereas glucose level remained unchanged (Fig. 2E). The MSC-CM dose of 2 mg/kg/day was considered suitable because our preliminary study showed that 1 mg/kg/day was not effective, whereas 4 mg/kg/day proved toxic and caused loss of body weight (data not shown). Injection of MSC-CM caused no fever in mice.

MSC and MSC-CM Therapies Prevented Histopathological Damage in Liver of HFD- and STZ-Diabetic Mice. Significant infiltration of inflammatory cells into the periportal area and numerous deposition of lipid droplets, which had a round vacuolar appearance, in hepatocytes were detected in HFD-vehicle mice (Fig. 1F). These pathological findings were attenuated in HFD-MSC and HFD-MSC-CM mice. Whereas massive accumulation of inflammatory cells in the periportal area and destruction of the round ligament of the liver were observed in STZ-vehicle mice (Fig. 2F), MSC and MSC-CM therapy suppressed excessive infiltration of inflammatory cells and reversed the structure of hepatic tissue.

MSC and MSC-CM Therapies Suppressed Excessive Infiltration of BMDCs, Especially Macrophages, in Liver of HFD- and STZ-Diabetic Mice. Areas occupied by BMDCs (green) were significantly larger in HFD- and STZ-vehicle mice, compared to controls (Figs. 3A and 4A, left). BMDCs massively infiltrated not only the hepatic sinusoid, but also the liver parenchyma and sometimes encircled hepatocytes. MSC and MSC-CM therapies reversed the increase in the quantitative area occupied by infiltrated BMDCs in liver of HFD- and STZ-vehicle mice (Figs. 3A and 4A, right).

We investigated the population of macrophages, which expressed F4/80 in BMDCs of diabetic liver. Infiltration of BM-derived macrophages (Figs. 3B and 4B, yellow) was remarkably increased in HFD- and STZ-vehicle mice, but was reversed to normal levels by MSC and MSC-CM therapies.

MSC and MSC-CM Therapies Modified the Character of BMDCs Infiltrating Liver and Mononuclear Cells in Peripheral Blood of HFD- and STZ-Diabetic Mice. Expression of interleukin (*Il*)-*6* and *Cd11c*, markers for classically activated macrophages, was unchanged in HFD-vehicle mice, compared to controls, although MSC and MSC-CM therapies down-regulated *Cd11c* expression (Fig. 3C). *Il-6* and *Cd11c* expression was up-regulated in STZ-vehicle mice, but was suppressed by MSC and MSC-CM therapies (Fig. 4C). Expression of *Fizz1* (found in inflammatory zone 1) and *Mrc1* (mannose receptor C type 1), markers for alternatively activated macrophages, was significantly decreased in HFD- and STZ-vehicle mice, compared to controls, but was reversed to normal levels or up-regulated by MSC and MSC-CM therapies (Figs. 3C and 4C).

MSC and MSC-CM Therapies Regulated Interaction Between BMDCs and Endothelial Cells in the Liver. Intracellular adhesion molecule 1 (ICAM-1) was stained in hepatic sinusoidal endothelial cells (HSECs), particularly in the periportal area in controls. Staining intensity was notably increased in HFD- and STZ-vehicle mice, but was decreased to control levels by MSC and MSC-CM therapies (Figs. 3D and 4D). Expression of *Ccr2* (C-C chemokine receptor 2), a receptor for monocyte chemotactic protein (MCP)−1, in GFP-positive BMDCs in the liver was significantly increased in HFD- and STZ-vehicle mice, compared to controls, in which *Ccr2* had been reversed to an almost normal level by MSC and MSC-CM therapies (Figs. 3E and 4E). Furthermore, expression of *Ccr2* in

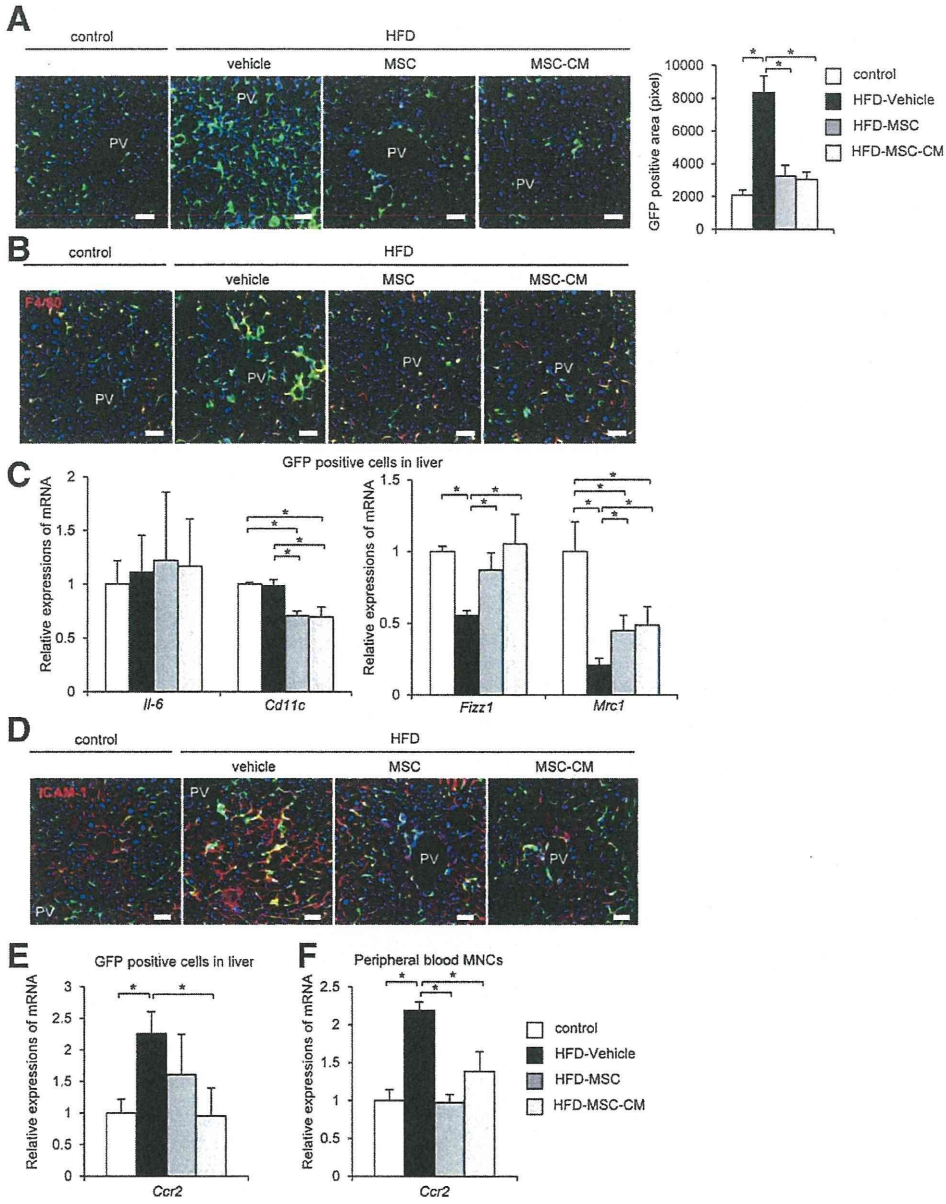

Fig. 3. BMDCs infiltrating liver of GFP-chimeric HFD-diabetic mice. (A) GFP-expressing BMDCs in the liver. GFP-positive density in the liver is quantified in right panel (mean value of 20 panels per group). (B) Immunofluorescence staining of F4/80 (red) in the liver. (C) mRNA expression of *Il-6*, *Cd11c*, *Fizz1*, and *Mrc1* on GFP-positive BMDCs in the liver. (D) Immunofluorescence staining of ICAM-1 (red) in the liver. mRNA expression of *Ccr2* on GFP-positive BMDCs in the liver (E) and PBMCs (F). Relative amounts of mRNA are normalized to an internal control, β-actin. Bar, 50 μm. Data are expressed as mean $\pm$ SE values of 5-8 animals. $^*P < 0.05$. mRNA, messenger RNA.

circulating mononuclear cells in peripheral blood of HFD- and STZ-vehicle mice was significantly increased, but MSC and MSC-CM therapies again reversed this increase (Figs. 3F and 4F).

MSC and MSC-CM Therapies Suppressed Proinflammatory Cytokine/Chemokine Expression in Liver of HFD- and STZ-Diabetic Mice. Inflammatory molecules, such as TNFα, MCP-1, and Toll-like receptor 4 (TLR4), were densely stained in both hepatocytes and BMDCs of HFD- and STZ-vehicle mice, and the staining was remarkably decreased by MSC and MSC-CM therapies (Figs. 5A and 6A). Fatty-acid-binding protein 4 (FABP4) was expressed in both sinusoidal endothelial cells (SECs) and hepatocytes of HFD-vehicle mice, and the staining intensity in hepatocytes was decreased by MSC and MSC-CM

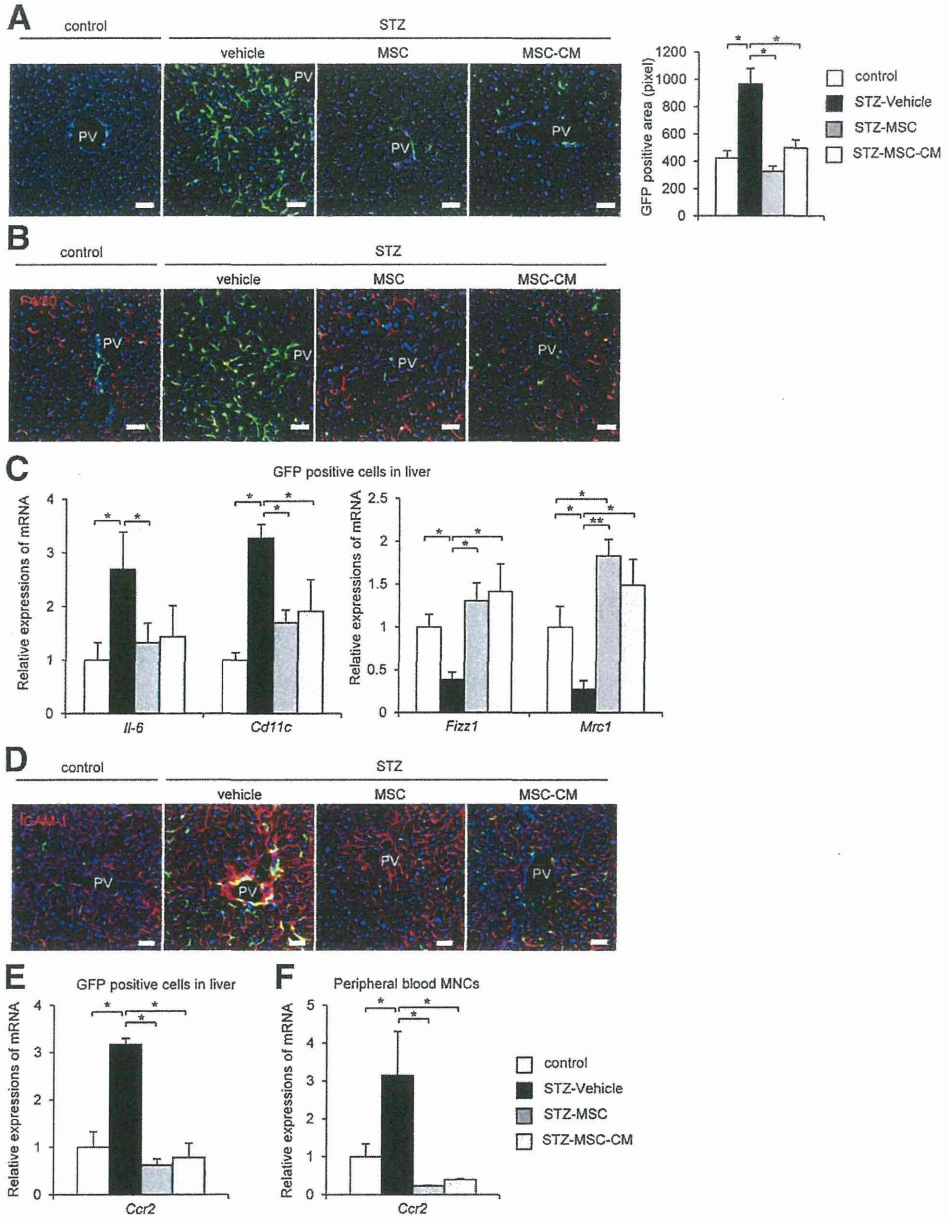

Fig. 4. BMDCs infiltrating liver of GFP-chimeric STZ-diabetic mice. (A) GFP-expressing BMDCs in the liver. GFP-positive density in the liver is quantified in right panel (mean value of 20 panels per group). (B) Immunofluorescence staining of F4/80 (red) in the liver. (C) mRNA expression of *Il-6*, *Cd11c*, *Fizz1*, and *Mrc1* on GFP-positive BMDCs in the liver. (D) Immunofluorescence staining of ICAM-1 (red) in the liver. mRNA expression of *Ccr2* on GFP-positive BMDCs in the liver (E) and PBMCs (F). Relative amounts of mRNA are normalized to an internal control, β-actin. Bar, 50 μm. Data are expressed as mean ± SE values of 5-9 animals. $^*P < 0.05$. mRNA, messenger RNA.

therapies (Fig. 5A). The receptor for advanced glycation endproducts was also densely stained in hepatocytes of STZ-vehicle mice, but staining intensity was decreased by MSC and MSC-CM therapies (Fig. 6A).

MSC and MSC-CM Therapies Regulated Inflammation, Proliferation, and Survival Signaling of Hepatocytes in HFD- and STZ-Diabetic Mice. Phosphorylation of c-Jun amino-terminal kinases (JNKs) and p38 mitogen-activated protein kinase (MAPK) was activated in liver of HFD- and STZ-vehicle mice (Figs. 5B, 6B), whereas activation of extracellular signal-regulated kinase (ERK)1/2 and protein kinase B (Akt) was suppressed in the liver (Figs. 5C and 6C). MSC and MSC-CM therapies reversed these alterations in both HFD- and STZ-diabetic mice.